2011

# G-protein betagamma-complex is crucial for efficient signal amplification in vision

Alexander V. Kolesnikov
*Washington University School of Medicine in St. Louis*

Loryn Rikimaru
*Saint Louis University*

Anne K. Hennig
*Washington University School of Medicine in St. Louis*

Peter D. Lukasiewicz
*Washington University School of Medicine in St. Louis*

Steven J. Fliesler
*Veterans Administration Western New York Healthcare System*

*See next page for additional authors*

Recommended Citation

**Authors**

Alexander V. Kolesnikov, Loryn Rikimaru, Anne K. Hennig, Peter D. Lukasiewicz, Steven J. Fliesler, Victor I. Govardovskii, Vladimir J. Kefalov, and Oleg G. Kisselev

Cellular/Molecular

# G-Protein $\beta\gamma$-Complex Is Crucial for Efficient Signal Amplification in Vision

**Alexander V. Kolesnikov,**[1] **Loryn Rikimaru,**[2] **Anne K. Hennig,**[1] **Peter D. Lukasiewicz,**[1] **Steven J. Fliesler,**[4,5,6,7] **Victor I. Govardovskii,**[8] **Vladimir J. Kefalov,**[1] **and Oleg G. Kisselev**[2,3]

[1]Department of Ophthalmology and Visual Sciences, Washington University School of Medicine, St. Louis, Missouri 63110, Departments of [2]Ophthalmology and [3]Biochemistry and Molecular Biology, Saint Louis University School of Medicine, Saint Louis, Missouri 63104, [4]Research Service, Veterans Administration Western New York Healthcare System, and Departments of [5]Ophthalmology (Ross Eye Institute) and [6]Biochemistry, University at Buffalo/The State University of New York (SUNY), and [7]SUNY Eye Institute, Buffalo, New York 14215, and [8]Sechenov Institute for Evolutionary Physiology and Biochemistry, Russian Academy of Sciences, Saint Petersburg 194223, Russia

A fundamental question of cell signaling biology is how faint external signals produce robust physiological responses. One universal mechanism relies on signal amplification via intracellular cascades mediated by heterotrimeric G-proteins. This high amplification system allows retinal rod photoreceptors to detect single photons of light. Although much is now known about the role of the $\alpha$-subunit of the rod-specific G-protein transducin in phototransduction, the physiological function of the auxiliary $\beta\gamma$-complex in this process remains a mystery. Here, we show that elimination of the transducin $\gamma$-subunit drastically reduces signal amplification in intact mouse rods. The consequence is a striking decline in rod visual sensitivity and severe impairment of nocturnal vision. Our findings demonstrate that transducin $\beta\gamma$-complex controls signal amplification of the rod phototransduction cascade and is critical for the ability of rod photoreceptors to function in low light conditions.

## Introduction

Retinal rod photoreceptors rely on the prototypical GPCR-mediated pathway to detect light (Stryer, 1986). They present a unique opportunity to address the physiological roles of individual subunits of heterotrimeric G-proteins because their phototransduction cascade is mediated by a single G-protein transducin (Gt) that consists of Gt$\alpha_1$ (Gt$\alpha$), Gt$\beta_1$ (Gt$\beta$), and Gt$\gamma_1$ (Gt$\gamma$) isoforms. Photoactivated rhodopsin (R*) binds to Gt and activates it by triggering the exchange of GDP for GTP on Gt$\alpha$. On activation, the G-protein dissociates into Gt$\alpha$-GTP and Gt$\beta\gamma$. In turn, Gt$\alpha$-GTP activates the effector enzyme phosphodiesterase (PDE6), which hydrolyzes cGMP. The resulting closure of cGMP-gated channels on the plasma membrane of the photoreceptor outer segment hyperpolarizes the cell and produces the light response. The activation of Gt represents the first amplification step in the rod phototrans-

duction cascade. In rods, a single R* molecule activates 20–100 Gt molecules during its lifetime (Leskov et al., 2000; Heck and Hofmann, 2001; Krispel et al., 2006). The resulting overall amplification allows rods to achieve the highest physically possible sensitivity and detect a single photon of light (Baylor et al., 1979).

Phototransduction in rods is mediated exclusively by Gt$\alpha$, as its deletion completely abolishes rod-driven photoresponse (Calvert et al., 2000). In contrast, the Gt$\beta\gamma$ complex has no established role in phototransduction *in vivo*. Early biochemical studies have suggested that Gt$\beta\gamma$ might participate in transducin activation (Fung, 1983). However, although it is now believed that Gt$\beta\gamma$ is necessary for maintaining the inactive state of Gt$\alpha$ and facilitating heterotrimer interactions with R* (Oldham and Hamm, 2008; Wensel, 2008), these conclusions are based on *in vitro* experiments performed under unphysiological conditions, with protein concentrations 1000-fold less (micromolar range) compared with those found in intact rods (Fu and Yau, 2007; Nickell et al., 2007). Furthermore, several biochemical experiments have suggested that, although effective R*-Gt coupling depends on the $\beta\gamma$-complex at low concentrations of rhodopsin, at higher bleached pigment concentrations, this dependence is lost and maximal activation of Gt$\alpha$ could be achieved without Gt$\beta\gamma$ (Navon and Fung, 1987; Phillips et al., 1992; Kisselev et al., 1999; Herrmann et al., 2006). Thus, it remains an open question whether Gt$\beta\gamma$ is required for effective signal amplification in intact rods, and the physiological role of the Gt$\beta\gamma$ complex in vision is still unclear. An earlier attempt to address this question using a commercially available (Deltagen) Gt$\gamma$ knock-out mouse strain was hampered by early onset of photoreceptor degeneration, which complicated its biochemical and physiological anal-

ysis, and resulted in the conclusion that Gtβγ does not have any specific role in visual signaling (Lobanova et al., 2008). Here, we used a different approach to create Gtγ-deficient mice with no discernable retinal degeneration during the early stages of postnatal life. Our behavioral, physiological, and biochemical analysis of these mice demonstrates that Gtβγ is crucial for the high amplification of the signaling cascade in intact rods required to support the high sensitivity of rod-mediated night vision.

## Materials and Methods

*Generation of* Gngt1 *knock-out mice.* All experiments were performed in accordance with the policy on the Use of Animals in Neuroscience Research and were approved by the Saint Louis University Institutional Animal Care and Use Committee and the Washington University Animal Studies Committee. Unless otherwise specified, all mice were age-matched 2- to 3-month-old littermates of either sex; they were kept under the standard 12 h dark/light cycle and dark-adapted overnight before all experiments.

The mouse rod Gtγ gene, *Gngt1*, was isolated and mapped by screening the mouse phage library. It contains three exons and two introns (Hurley et al., 1984; Yatsunami et al., 1985; Tao et al., 1993; Scherer et al., 1996; Downes and Gautam, 1999) (see Fig. 1*A*). The targeting construct was designed to replace all three exons with a Neo cassette to eliminate the coding region of Gtγ. The conventional targeting vector was constructed by using a 1.6 kb DNA fragment as the short homology arm (SA). It was amplified by PCR using primers located 1.9 and 0.2 kb upstream of exon 1. SA was subcloned at the 5′-end of the Neo cassette in the 5′–3′ orientation using MluI sites. The long homology arm (LA), a 7.3 kb XbaI fragment isolated from a lambda phage clone, was inserted at the 3′-end of the Neo cassette in the 5′–3′ orientation using AvrII sites. The targeting vector was confirmed by restriction analysis and sequencing. This transgenic design is notably different from the commercially available Deltagen *Gngt1*$^{-/-}$ mouse (Deltagen; target ID 408), in which *Gngt1* was targeted by a gene trap replacement of a part of the Gtγ coding sequence (amino acids 17–44) and intron 2 by the IRES-LacZ-Neo cassette.

The *Gngt1* knock-out construct was electroporated into the 129 strain of ES cells, and G418-resistant clones were identified by PCR, DNA sequencing, and Southern blotting (inGenious Targeting Laboratory). Positive clones were injected into blastocysts to generate chimeric mice. Germline transmission in F$_1$ and in subsequent generations derived by crossings with C57BL/6 was confirmed by PCR using primers A1/N1 for the 1.8 kb knock-out (KO) allele and WTi1/WTi2 for the 460 bp wild-type (WT) allele (data not shown). The forward A1 primer (5′-GGAGAACACTCATGGAGA-AGCTC-3′) was just outside of SA, and the reverse N1 primer (5′-CCAGAGGCCACTTGTGTAGC-3′) was within the Neo gene. The forward WTi1 primer (5′-GTAAGTGCAAAGCAGAGGCATGGGCTGCCTG-TGGGCTC-3′) was inside intron 1, and the reverse WTi2 primer (5′-CCCGATCCAAGTGTGGCTCTTTGCCTGTTTTGGTACGAC-3′) was inside intron 2.

*Antibodies and Western blotting.* Rabbit antibodies sc-389-Gtα$_1$, sc-390-Gtα$_2$, sc-380-Gβ$_2$, sc-381-Gβ$_3$, sc-374-Gγ$_2$, sc-375-Gγ$_3$, sc-376-Gγ$_5$, sc-377-Gγ$_7$, sc-15382-rhodopsin, sc-28850-phosducin, as well as goat antibodies sc-26776-Gγ$_4$, sc-8143-RGS9, and mouse antibodies sc-8004-GRK1, sc-73044-SNAP25 were from Santa Cruz Biotechnology. Rabbit antibodies against Gγ$_c$ and PDEα, PDEβ, and PDEγ were from CytoSignal Research Products. Rabbit antibodies against GCAP1, GCAP2, and retGC1 were a gift from A. M. Dizhoor (Pennsylvania College of Optometry, Elkins Park, PA). Rabbit antibodies against M-opsin and S-opsin were a gift from C. M. Craft (Zhu et al., 2003) (Mary D. Allen Laboratory for Vision Research, Doheny Eye Institute, University of Southern California, Los Angeles, CA). Rabbit antibodies against Gβ$_1$ and Gγ$_1$ were a gift from N. Gautam (Washington University, St. Louis, MO). Rabbit Gβ$_5$ antibody was a gift from W. F. Simonds (National Institute of Diabetes and Digestive and Kidney Diseases, Bethesda, MD). Mouse antibody for rod arrestin was a gift from W. C. Smith (University of Florida, Gainesville, FL). Rabbit antibody against PhLP was a gift from B. M. Willardson (Brigham Young University, Provo, UT). Rabbit anti-

body AB5585-recoverin was from Millipore. Secondary HRP antibodies were from Jackson ImmunoResearch Laboratories. Blots were developed using Pierce Femto Supersignal kit. Signal intensity of the protein bands on x-ray film was quantified by densitometry using Image Gauge (FujiFilm).

*Light microscopy, electron microscopy, and immunohistochemistry.* For immunolabeling, eyes were fixed in freshly prepared 0.1 M phosphate buffer, pH 7.4, containing 2% paraformaldehyde and 0.1% glutaraldehyde and embedded in LR White. Semithin 0.5 μm sections were cut in the dorsal-to-ventral direction through the optic nerve and immunostained essentially as previously described (Naash et al., 2004) followed by silver intensification using an IntenSE M Silver Enhancement Kit (GE Healthcare). For electron microscopy, ultrathin 0.1 μm sections were picked up on uncoated 75/300 mesh nickel grids, stained with uranyl acetate and lead citrate, and exposed to OsO$_4$ vapor for 30 min.

For measurements of rod outer segment (ROS) length, the embedded blocks were sectioned in the dorsal-to-ventral direction through the optic nerve. Twenty independent measurements were made starting at ~500 μm from the edge of the optic nerve head on both sides with 2 μm steps between individual measurements, and the mean and SEM values were calculated for each specimen.

*Protein quantification and transducin membrane partitioning.* Retinas and ROS disk preparations used for Western blotting were from 2-month-old mice. Dark-adapted mouse ROS disc membranes were prepared from 50 to 150 mouse retinas, as previously described (Papermaster and Dreyer, 1974). Purified ROS disk membrane pellets contained only membrane-bound transducin subunits. They were aliquoted and stored at −80°C until protein quantification or biochemical experiments. Soluble transducin fraction was lost during the ROS disk membrane purification procedure and thus was not considered in additional analysis. Contamination by the inner segment marker, cytochrome *c*, was undetectable. Bovine Gtα and Gtβγ subunits were purified and total ROS disk membrane protein and rhodopsin concentration were measured as previously described (Kisselev, 2007). Using rhodopsin or total ROS disk membrane protein measurements as loading controls produced similar results.

For partitioning experiment, R*-Gt binding measurements in fully bleached ROS disk membranes were performed as described previously (Kisselev, 2007), with the following modifications: mouse ROS disk membrane pellets were resuspended at 3 μM rhodopsin in 10 mM Tris-HCl, pH 7.4, 100 mM NaCl, 5 mM MgCl$_2$, 1 mM DTT, and 0.1 mM PMSF, to establish a new equilibrium between the membrane and soluble Gt. After light activation, samples were incubated on ice for 10 min, and supernatant and pellet were separated by centrifugation at 100,000 × *g* at 4°C for 10 min in a TLA-100.3 rotor. Gtα content in both fractions was analyzed by quantitative immunoblotting.

*Electroretinography.* Animals were dark-adapted overnight and anesthetized by subcutaneous injection of ketamine (80 mg/kg) and xylazine (15 mg/kg). Pupils were dilated with 1% atropine sulfate. During testing, a heating pad controlled by a rectal temperature probe maintained body temperature at 37–38°C. Full-field ERGs were recorded using a UTAS-E3000 apparatus (LKC Technologies) and platinum corneal electrodes, as described (Brantley et al., 2008; Kolesnikov et al., 2010). Reference and ground electrode needles were inserted under the skin at the skull and the tail, respectively. Test flashes of 15–650 μs white light were applied either in darkness (scotopic conditions) or in the presence of steady background illumination (200 cd m$^{-2}$), after 5 min adaptation to the background light (photopic conditions). Responses from several trials were averaged and the intervals between trials were adjusted so that responses did not decrease in amplitude over the series of trials for each step. The recorded responses were bandpass filtered at 0.05–1500 Hz.

*Single-cell electrophysiology.* In contrast to the previously characterized Deltagen *Gngt1*$^{-/-}$ model (Lobanova et al., 2008), suction recordings could be performed easily from the rods of our 2- to 3-month-old *Gngt1*$^{-/-}$ mice because of the lack of early retinal degeneration. Animals were dark-adapted overnight and the retinas were removed, chopped into small pieces, and transferred to a perfusion chamber. A single rod outer segment was drawn into a glass microelectrode filled with solution containing 140 mM NaCl, 3.6 mM KCl, 2.4 mM MgCl$_2$, 1.2 mM CaCl$_2$, 3

mM HEPES, pH 7.4, 0.02 mM EDTA, and 10 mM glucose. The perfusion solution contained 112.5 mM NaCl, 3.6 mM KCl, 2.4 mM MgCl₂, 1.2 mM CaCl₂, 10 mM HEPES, pH 7.4, 20 mM NaHCO₃, 3 mM Na succinate, 0.5 mM Na glutamate, 0.02 mM EDTA, and 10 mM glucose. The perfusion solution was bubbled with 95% O₂/5% CO₂ mixture and heated to 37–38°C.

Light stimulation was applied by 20 ms test flashes of calibrated 500 nm light. Photoresponses were amplified, low-pass filtered (30 Hz, 8-pole Bessel), and digitized (1 kHz). Dominant recovery time constant ($\tau_D$) was determined from supersaturating flashes (Pepperberg et al., 1992), using a 10% criterion for photocurrent recovery from saturation. The amplification of the rod phototransduction cascade was evaluated from test flash intensities that produced identical rising phases of dim flash responses. This approach was preferred to the Lamb and Pugh determination of the amplification constant (Pugh and Lamb, 1993) because of the relatively long duration of test flashes and the effect of low-pass filtering on the response front.

*Spatial contrast sensitivity measured from optomotor responses.* Spatial contrast visual sensitivity of age-matched 2- to 3-month-old mice was measured using a two-alternative forced-choice protocol (Umino et al., 2008). The Optomotry system (Cerebral Mechanics) consisted of a square array of four computer monitors with a pedestal in the center where the mouse was placed. An infrared-sensitive television camera and a round array of six infrared LEDs mounted above the animal were used to observe the mouse but not the monitors. Using a staircase paradigm, rotating stimuli (sine wave vertical gratings) were applied on the monitors where they formed a virtual cylinder around the mouse (Prusky et al., 2004). Mice responded to the stimuli by reflexively rotating their head in the corresponding direction. Contrast sensitivity was defined as the inverse of contrast threshold for optomotor responses. Responses were measured over a range of background light intensities, from −6.25 to 1.85 log cd m⁻². Background monitor luminance was controlled by neutral density film filters (E-Color 211 0.9 ND; Rosco Laboratories). Temporal frequency ($f_t$) was fixed at its optimal value of 0.75 Hz for all background conditions. Spatial frequency ($f_s$) was varied in the range of 0.014–0.481 cyc/deg, and speed of the stimuli was adjusted based on the following equation: $f_t = s_p \cdot f_s$ (Umino et al., 2008). For determination of maximal contrast sensitivity under each condition, data were fitted with mouse contrast sensitivity model (Umino et al., 2008), using parameters adjusted for best fit ($r^2 > 0.8$). All data were analyzed using independent two-tailed Student's $t$ test, with accepted significance level of $p < 0.05$.

*Mathematical modeling of phototransduction.* A mathematical model of phototransduction (Kuzmin et al., 2004) was used. This model includes all firmly established biochemical mechanisms of phototransduction and its regulation by calcium feedback. Basic equations of the model are similar to those used in many previous works (Hamer, 2000a,b; Nikonov et al., 2000; Hamer et al., 2003, 2005). However, our treatment of Ca²⁺ regulation and Ca²⁺ turnover differs slightly from that used before. Therefore, we present here the full set of equations comprising the model.

Number of active rhodopsin molecules, $R^*$, is determined by a balance between its generation by light, $I(t)$, and quenching by phosphorylation with rhodopsin kinase. We omit the detailed description of Ca²⁺ regulation of rhodopsin kinase via recoverin (Hamer et al., 2003, 2005) and instead use an empirical Hill-like relationship (the term in parentheses on right side of Eq. 1) (Calvert et al., 1998) as follows:

$$\frac{dR^*(t)}{dt} = I(t) - \left( k_{Rmin} + \frac{k_{Rmax} - k_{Rmin}}{1 + (Ca(t)/K_{CaR})^{n_{CaR}}} \right) \cdot R^*(t). \quad (1)$$

Here, $k_{Rmin}$ and $k_{Rmax}$ are minimum and maximum rate constants of phosphorylation (in seconds⁻¹) at very high and zero Ca²⁺ concentrations, respectively. $K_{CaR}$ is the half-saturating Ca²⁺ concentration, and $n_{CaR}$ is the Hill's coefficient of regulation.

Number of activated phosphodiesterase molecules $E^*$ is given by the following:

$$\frac{dE^*(t)}{dt} = \nu_{RE}R^*(t) - k_E E^*(t), \quad (2)$$

where $\nu_{RE}$ is the rate of PDE activation by single $R^*$ (in seconds⁻¹), and $k_E$ is the rate constant of $E^*$ turnoff (in seconds⁻¹).

cGMP turnover is described by the following:

$$\frac{dcG(t)}{dt} = \alpha(t) - \beta(t), \quad (3)$$

where $\alpha(t)$ is the rate of cGMP production by guanylate cyclase, and $\beta(t)$ is the rate of its hydrolysis by phosphodiesterase. Here, cGMP concentration is expressed in moles · liter⁻¹, and $\alpha(t)$ and $\beta(t)$, in moles · liter⁻¹ · second⁻¹.

Guanylate cyclase activity is under calcium control, in the form similar to that for $R^*$ turnoff as follows:

$$\alpha(t) = \alpha_{min} + \frac{\alpha_{max} - \alpha_{min}}{1 + (Ca(t)/K_{cyc})^{n_{cyc}}}. \quad (4)$$

Notice that, in this formulation, like in the study by Nikonov et al. (2000) (Eq. A10), the extent of guanylate cyclase regulation is limited by the range between $\alpha_{max}$ and $\alpha_{min}$, in contrast to most recent models (Burns et al., 2002; Hamer et al., 2003, 2005) that assume infinite regulation range ($\alpha_{min} = 0$).

The rate of cGMP hydrolysis is as follows:

$$\beta(t) = \left( \beta_{Dark} + \frac{k_{cat}}{V_{cyto}N_{A\nu}}E*(t) \right) \frac{cG(t)}{cG(t) + K_m}. \quad (5)$$

Here, $\beta_{Dark}$ is the steady PDE activity in darkness, and the second term in parentheses yields light-induced activity. $k_{cat}$ is the catalytic activity of a single light-activated PDE subunit (in seconds⁻¹), whereas ROS cytoplasmic volume $V_{cyto}$ and Avogadro's number $N_{Av}$ convert the number of photoactivated PDE molecules into concentration. Hydrolysis of cGMP is supposed to proceed in accordance with Michaelis kinetics, with the half-saturating cGMP concentration $K_m$. Again, we do not make the simplifying assumption $cG(t) \ll K_m$ common in recent models.

The ROS membrane current is a sum of two components, the current flowing through cGMP-gated channels $j_{cG}(t)$ and the current carried by the Ca,Na/K exchanger $j_{ex}(t)$:

$$j_{cG}(t) = j_{cGmax} \frac{cG(t)^{n_{cG}}}{cG(t)^{n_{cG}} + K_{cG}^{n_{cG}}} + j_{ex}(t), \quad (6)$$

where $j_{cGmax}$ is maximum current at saturating cGMP concentrations, $K_{cG}$ is a half-saturating concentration, and $n_{cG}$ is the Hill's coefficient of the regulation of the channels.

Free Ca²⁺ turnover is described by the following:

$$\frac{dCa(t)}{dt} = \frac{1}{FB + 1} \left( \frac{(1/2) \cdot f_{Ca} j_{cG}(t) - j_{ex}(t)}{\Im \cdot V_{cyto}} \right.$$
$$\left. - k_{+1} \cdot Ca(t)(B_{max} - Ca_{Bslow}(t)) + k_{-1} \cdot Ca_{Bslow}(t) \right). \quad (7)$$

Here, $f_{Ca}$ is the fraction of the ROS current carried by Ca²⁺, $j_{ex}$ is Ca²⁺ extrusion current carried by Ca,K/Na exchanger, and $\Im$ is Faraday's number [cf. Hamer et al. (2005), their Eq. A9]. In accordance with experimental data on amphibian rods (McCarthy et al., 1996; Younger et al., 1996; Govardovskii and Kuzmin, 1999), ROSs are supposed to contain a two-component Ca²⁺ buffer. One of the components exchanges with free Ca²⁺ quickly, so its effect on free Ca²⁺ turnover can simply be characterized by its buffering power, FB (Lagnado et al., 1992). The second, slowly exchangeable component is characterized by its binding capacity $B_{max}$, and two rate constants, $k_{+1}$ for binding and $k_{-1}$ for releasing Ca²⁺. $Ca_{Bslow}(t)$ is the concentration of calcium bound to slow buffer and is described by the following:

$$\frac{dCa_{Bslow}(t)}{dt} = k_{+1} \cdot Ca(t)(B_{max} - Ca_{Bslow}(t)) - k_{-1} \cdot Ca_{Bslow}(t). \quad (8)$$

**Table 1. Experimental parameters of single-cell responses and model parameters that were varied to simulate the effects of Gtγ deletion on flash responses**

| | Wild type (n = 50) | Gngt1^{+/−} (n = 27) | Gngt1^{−/−} (n = 41) |
|---|---|---|---|
| **Response parameter** | | | |
| $I_{dark}$ (pA) | 15.7 ± 0.3 | 14.9 ± 0.4[NS] | 14.9 ± 0.3[NS] |
| $I_{1/2}$ (ph $\mu m^{-2}$) | 93 ± 2 | 130 ± 10** | 8408 ± 553** |
| $T_{peak}$ (ms) | 152 ± 2 | 121 ± 2** | 99 ± 2** |
| $T_{integr}$ (ms) | 260 ± 9 | 246 ± 14[NS] | 132 ± 5** |
| $\tau_{rec}$ (ms) | 190 ± 10 | 184 ± 13[NS] | 121 ± 5** |
| $\tau_D$ (ms) | 200 ± 13 (16) | 161 ± 10 (19)** | 141 ± 9 (23)** |
| **Model parameter** | | | |
| $\nu_{RE}$ ($s^{-1}$) | 307 | 305 | 9.4 |
| $k_{Rmax}$ ($s^{-1}$) | 11.4 | 22.3 | 63.5 |
| $k_E$ ($s^{-1}$) | 6.5 | 5.4 | 8.3 |
| FB | 59.4 | 32.1 | 30.1 |

Values are means ± SEM. Experimental parameters were as follows: $I_{dark}$, Dark current measured from saturated responses; $I_{1/2}$, half-saturating light intensity; time-to-peak ($T_{peak}$) and integration time ($T_{integr}$) refer to responses whose amplitudes were <0.2$I_{dark}$ and fell within the linear range; $\tau_{rec}$, time constant of single-exponential decay of dim flash response recovery phase; $\tau_D$, dominant time constant of recovery after supersaturating flashes determined from the linear fit to time in saturation versus intensity semilog plots (Pepperberg et al., 1992). Model parameters were as follows: $\nu_{RE}$, rate of PDE activation by single R*; $k_{Rmax}$, maximum rate constant of R* turnoff at zero Ca$^{2+}$$_{in}$; $k_E$, rate constant of PDE* turnoff; FB, buffering power of fast Ca$^{2+}$ buffer. Values were determined for population-averaged dim flash responses normalized to amplitudes of corresponding saturated responses.

[NS]$p > 0.05$; **$p < 0.001$ compared with wild-type values.

In the present paper, we set $B_{max} = 0$ (see Table 2). With properly chosen FB, this does not significantly affect the quality of fitting of flash responses but reduces the number of free model parameters.

The exchanger current is described in Michaelis' manner (Cervetto et al., 1989) as follows:

$$j_{ex}(t) = j_{exsat} \frac{Ca(t)}{Ca(t) + K_{ex}}. \tag{9}$$

The parameters of the model were chosen to be within empirical biochemical and biophysical values when such data were available (Tables 1, 2). This provided a great flexibility of fitting, allowing virtually perfect simulation of photoresponses (coefficient of correlation between experimental and model traces $r > 0.999$ in wild-type and Gngt1$^{−/−}$ rods, and $r > 0.997$ in Gngt1$^{+/−}$ rods). However, our goal was not to produce the best fit of the experimental data, but rather to determine what parameters of the phototransduction cascade must be modified to account for the effects of Gtγ deletion. Thus, a group of parameters that was unlikely to be affected by the lack of Gtγ was kept constant among wild-type, Gngt1$^{+/−}$, and Gngt1$^{−/−}$ rods. These included properties of the ROS plasma membrane, namely, surface density, ionic selectivity, and affinity to cGMP of the cGMP-gated channels, and properties of the Ca$^{2+}$,K$^+$/Na$^+$ exchanger. Since the dark current was virtually unchanged in genetically manipulated rods, the above assumptions imply that the dark concentrations of cGMP and Ca$^{2+}$ also remained constant. Although a constant dark cGMP level does not necessary mean that dark guanylate cyclase and phosphodiesterase activities remained unchanged, the two parameters were fixed as well. Furthermore, parameters of the Ca$^{2+}$ modulation of the cascade components (fold regulation, affinities, and Hill's coefficients in Eqs. 1 and 4) were also kept constant.

For proper comparison with experimental responses, model curves were Gauss-filtered, with smoothing window of 23 ms equivalent to experimental 30 Hz Bessel filter.

## Results

### Lack of early retinal degeneration in Gtγ-deficient mice

To investigate the function of Gtβγ in the phototransduction pathway *in vivo*, we generated a mouse line lacking the retinal rod-specific Gtγ subunit (Gngt1$^{−/−}$) (Fig. 1A). Morphological and ultrastructural analysis of 1- to 2-month-old Gngt1$^{−/−}$ retinas by light microscopy (Fig. 1B) and transmission electron microscopy (data not shown) demonstrated normal retinal development and photoreceptor maturation. This result clearly

**Table 2. Definition of model parameters**

| Parameter | Meaning | Units | Value |
|---|---|---|---|
| $V_{cyto}$ | ROS cytoplasmic volume | l | $1.4 \cdot 10^{-14}$ |
| **Rhodopsin activation and quenching** | | | |
| $I$ | Light intensity | $R^* \cdot s^{-1}$ | |
| $R^*$ | Number of activated rhodopsin molecules | | |
| $k_{Rmax}$ | Maximum rate constant of $R^*$ inactivation | $s^{-1}$ | |
| $k_{Rmax}/k_{Rmin}$ | Fold regulation of the rate of $R^*$ inactivation | | 3.3 |
| $K_{CaR}$ | Half-saturating $Ca$ for $R^*$ inactivation | M | $5 \cdot 10^{-7}$ |
| $n_{CaR}$ | Hill's coefficient for $R^*$ inactivation control by $Ca$ | | 2.6 |
| **PDE activation and quenching** | | | |
| $E^*$ | Number of activated PDE molecules | | |
| $\nu_{RE}$ | Rate of PDE activation by fully active $R^*$ | $s^{-1}$ | |
| $k_E$ | Rate constant of PDE quenching | $s^{-1}$ | |
| **cGMP turnover** | | | |
| $cG$ | Concentration of free cGMP in darkness | M | $3 \cdot 10^{-6}$ |
| $\alpha_{min}$ | Minimum rate of cGMP synthesis | $M \cdot s^{-1}$ | $34.8 \cdot 10^{-8}$ |
| $\alpha_{max}$ | Maximum rate of cGMP synthesis | $M \cdot s^{-1}$ | $34.8 \cdot 10^{-6}$ |
| $K_{cyc}$ | Half-saturating $Ca$ for regulation of $\alpha$ | M | $4.8 \cdot 10^{-7}$ |
| $n_{cyc}$ | Hill's coefficient for $Ca$ regulation of $\alpha$ | | 3.5 |
| $\beta_{Dark}$ | Rate of cGMP hydrolysis in darkness | $M \cdot s^{-1}$ | $7 \cdot 10^{-5}$ |
| $k_{cat}$ | Catalytic activity of single PDE subunit | $s^{-1}$ | 2200 |
| $K_m$ | PDE's Michaelis constant | M | $10^{-5}$ |
| **Photocurrent control** | | | |
| $j_{cGdark}$ | Dark current | A | $1.5 \cdot 10^{-11}$ |
| $j_{cGmax}$ | Maximum ROS current at saturating $cG$ | A | $4.45 \cdot 10^{-9}$ |
| $n_{cG}$ | Hill's coefficient of cG channels activation by cGMP | | 3 |
| $K_{cG}$ | Half-saturating $cG$ for channels' activation | M | $2 \cdot 10^{-5}$ |
| **Ca$^{2+}$ turnover** | | | |
| $Ca$ | Cytoplasmic concentration of free Ca$^{2+}$ ions | M | $5 \cdot 10^{-7}$ |
| $f_{Ca}$ | Fraction of ROS current carried by Ca$^{2+}$ | | 0.16 |
| $j_{exsat}$ | Maximum exchanger current at saturating $Ca$ | A | $4.8 \cdot 10^{-12}$ |
| $K_{ex}$ | Half-saturating $Ca$ for the exchanger | M | $1.5 \cdot 10^{-6}$ |
| FB | Buffering power of fast Ca$^{2+}$ buffer | | |
| $B_{max}$ | Concentration of slow Ca$^{2+}$ buffer | M | 0 |
| $k_{+1}$ | Rate constant of Ca$^{2+}$ binding to slow buffer | $M^{-1}s^{-1}$ | NA |
| $k_{-1}$ | Rate constant of Ca$^{2+}$ release from slow buffer | $s^{-1}$ | NA |

Numerical values are given for the parameters that were kept constant in all three mouse strains.

indicates that the Gtβγ complex is not required for the formation of the rod outer segments. Although Gngt1$^{−/−}$ retinas showed slow progressive retinal degeneration with an onset at 3–4 months, this effect was negligible at early adult ages (Fig. 1C). Notably, the rate of late rod degeneration was similar to that observed in the Gtα-deficient (Gnat1$^{−/−}$) mice (Calvert et al., 2000) indicating that Gtγ- and Gtα-deficient rods are only weakly susceptible to degeneration. This result argues against the notion that Gtγ is critical for rod viability (Lobanova et al., 2008), which, in addition, may be influenced by the choice of targeting construct and genetic background of the mice.

We used retina extracts, as well as highly purified Gngt1$^{−/−}$ ROS disk membrane preparations, to analyze the protein composition of Gngt1$^{−/−}$ rods. The ROS disks contained no contamination by rod inner segment (RIS), as demonstrated by the absence of the RIS marker cytochrome c (cyt c) (Fig. 1D). Consistent with the normal retinal morphology of Gngt1$^{−/−}$ retinas, the deletion of Gtγ had no effect on the level of rhodopsin expression (Fig. 1E). As ex-
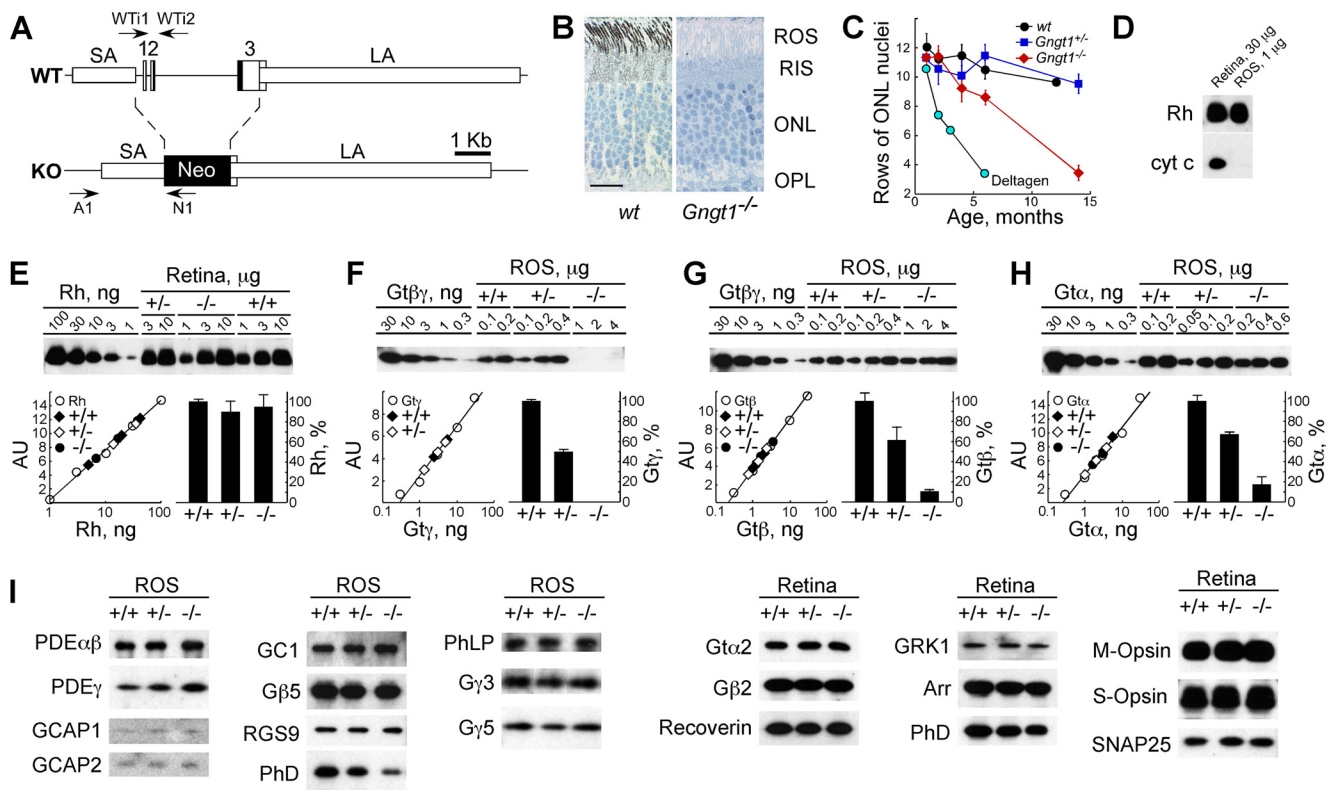
**Figure 1.** Genetic, morphological, and biochemical characterization of *Gngt1*$^{-/-}$ mice. ***A***, Schematic representation of WT and KO alleles. WT gene exons 1–3 are shown by tall white boxes. The Gt$\gamma$ protein coding region in exons 2 and 3 is shown in black. SA is the 1.6 kb short homology arm. LA is the 7.3 kb long homology arm. The 3.4 kb region of the *Gngt1* gene encompassing exons 1, 2, and 3 was replaced by 1.8 kb Neo cassette. For PCR genotyping, a 460 bp DNA fragment in the WT allele was amplified by WTi1 and WTi2 primers, and a 1.8 kb fragment in the KO allele was amplified by A1 and N1 primers (data not shown). The arrows show the position of the primers. ***B***, Immunostaining of wild-type and *Gngt1*$^{-/-}$ retinas with anti-Gt$\gamma$ antibody: immunogold staining with silver enhancement, LR white embedment, toluidine blue counterstaining. Scale bar, 20 $\mu$m. ***C***, Average number of rows of outer nuclear layer (ONL) nuclei (means $\pm$ SD; $n = 15$) as a function of age. The cyan circles (Deltagen) represent comparative data reconstituted from Figure 2 in the study by Lobanova et al. (2008). ***D***, Immunoblotting of whole retina extracts and purified ROS disk membranes from *Gngt1*$^{-/-}$ retinas using anti-opsin and anti-cytochrome *c* antibodies. The lack of cyt *c* in ROS membranes demonstrates that they were not contaminated with the RIS material. ***E–H***, Expression of retinal proteins determined by quantitative immunoblotting: rhodopsin in the retina (***E***); Gt$\gamma$ (***F***), Gt$\beta$ (***G***), and Gt$\alpha$ (***H***) in ROS disk membranes isolated from *Gngt1*$^{-/-}$ retinas. Levels of rhodopsin and transducin $\alpha$ and $\beta$ subunits in whole mouse retinas and ROS disk preparations were determined based on quantitative calibrations with highly purified bovine rhodopsin and transducin standards. The data represent means $\pm$ SD from three independent experiments. ***I***, Effects of Gt$\gamma$ deletion on the expression of phototransduction proteins in rods. Whole retina and ROS samples were prepared from 2-month-old wild-type, *Gngt1*$^{+/-}$, and *Gngt1*$^{-/-}$ mice. The sample rhodopsin level was used as a loading control for quantification of phototransduction proteins. Similar results were obtained when total protein was used as the loading control (data not shown).

pected, purified ROS were lacking Gt$\gamma$ (Fig. 1*F*). Because all G$\beta\gamma$ complexes function as nondissociable dimers, the deletion of Gt$\gamma$ resulted in a dramatic reduction in Gt$\beta$ as well, with only 10% remaining in *Gngt1*$^{-/-}$ rods (Fig. 1*G*). The level of Gt$\beta\gamma$ expression showed a clear gene titration effect, as the levels of Gt$\beta$ and Gt$\gamma$ subunits in *Gngt1*$^{+/-}$ ROS disks were reduced to 61 and 50%, respectively (Fig. 1*F,G*). Finally, we also observed a decrease in the levels of Gt$\alpha$ bound to dark-adapted *Gngt1*$^{+/-}$ and *Gngt1*$^{-/-}$ ROS disk membranes to 67 and 17%, respectively (Fig. 1*H*). A decrease of similar magnitude was also observed by immunohistochemical analysis of the *Gngt1*$^{-/-}$ retinas (data not shown). Notably, the ROS disk membrane-bound fraction of Gt$\alpha$ in our animals (17% of wild-type levels) was substantially higher than the expression of Gt$\alpha$ in the ROS of the commercial Deltagen *Gngt1*$^{-/-}$ mice (2%) (Lobanova et al., 2008). A possible reason for this prominent difference could be the significantly faster rate of retinal degeneration in the Deltagen *Gngt1*$^{-/-}$ mutant, even at very early ages.

Among 19 other major phototransduction proteins examined, all but phosducin and PDE$\gamma$ had expression levels similar to those in wild-type rods (Fig. 1*I*). Phosducin levels in retinas of *Gngt1*$^{+/-}$ and *Gngt1*$^{-/-}$ mice were downregulated to 83 and

62% of those in control retinas, respectively. ROS-localized phosducin was reduced even more dramatically, to 69 and 35%, respectively (Fig. 1*I*). This effect appears to be reciprocal to the observed reduction of the Gt$\beta\gamma$ expression in the phosducin knock-out mouse line (Krispel et al., 2007). Interestingly, we also observed an unexpected twofold and threefold increase in the levels of inhibitory PDE$\gamma$ subunit in *Gngt1*$^{+/-}$ and *Gngt1*$^{-/-}$ ROS, respectively (Fig. 1*I*). Finally, we consistently detected residual amounts of G$\gamma$3 and G$\gamma$5 in our ROS preparations, possibly because of contamination with ROS plasma membranes or other retinal subcellular elements. None of the following G$\gamma$ subunits were detected: G$\gamma_2$, G$\gamma_4$, G$\gamma_7$, G$\gamma_8$, G$\gamma_{10}$, G$\gamma_{11}$, G$\gamma_{12}$, and G$\gamma_{13}$ (data not shown). The lack of early retinal degeneration and the normal expression levels of most transduction proteins in our mice allowed us to quantitatively characterize how the deletion of Gt$\gamma$ affects their visual function as well as the phototransduction properties of individual rods.

## Impaired rod function in Gt$\gamma$-deficient mice
To determine how the deletion of Gt$\gamma$ affects the overall functionality of mouse vision, we first performed behavioral tests based on the ability of mice to reflexively respond to computer-
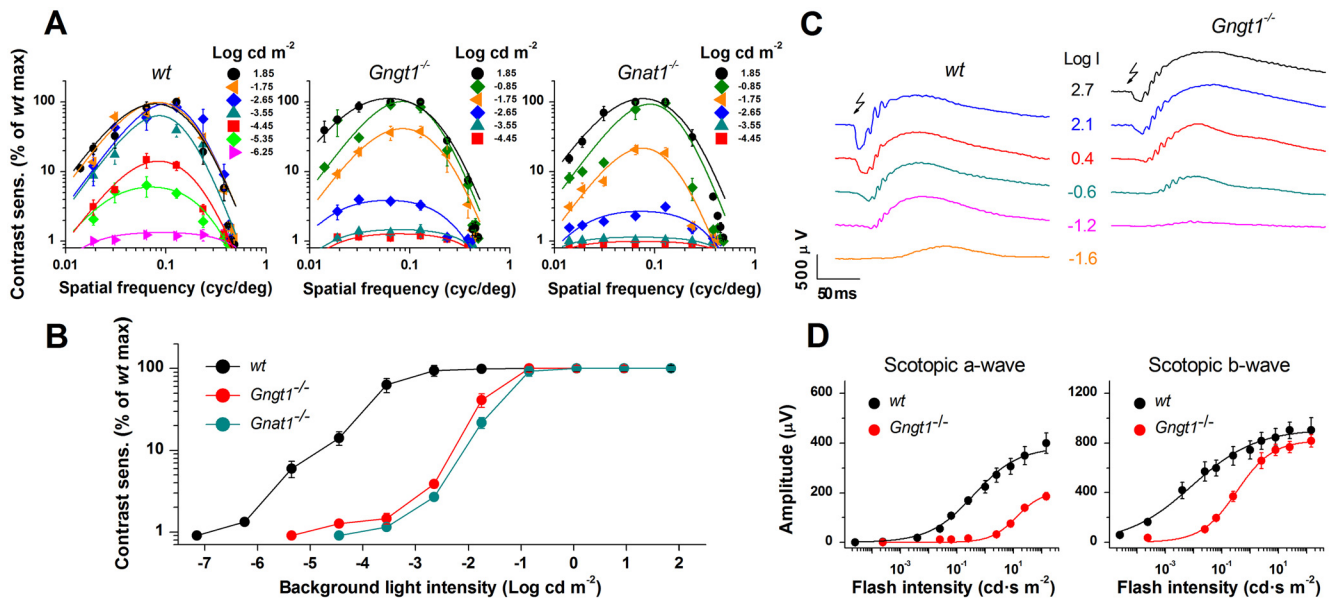
**Figure 2.** Impairment of visual function in Gtγ-deficient mice. **A**, Spatial contrast sensitivity functions (CSFs) of wild-type (left; n = 3), Gngt1 [−/−] (middle; n = 3), and Gnat1 [−/−] (right; n = 3) mice. Temporal frequency ($f_t$) was fixed at its optimal value of 0.75 Hz for all light intensities. To determine the maximal contrast sensitivity under each condition, data were fitted with a mouse contrast sensitivity model (Umino et al., 2008). All data points below unity indicate no detectable optomotor responses. **B**, Averaged amplitudes of spatial CSFs as functions of background light intensity. All values are means ± SEM (n = 3 for all groups). **C**, Families of ERG responses from wild-type (left) and Gngt1 [−/−] (right) animals. **D**, Intensity–response relationships for scotopic a-waves (left) and b-waves (right). Data were fitted with hyperbolic functions that yielded scotopic a-wave half-saturating light intensities of $0.39 \pm 0.08$ cd · s m^{−2} (wild type, n = 7) and $13.0 \pm 3.1$ cd · s m^{−2} (Gngt1 [−/−], n = 7), and a-wave maximum amplitudes of $382 \pm 41$ μV (wild type, n = 7) and $207 \pm 15$ μV (Gngt1 [−/−], n = 7). Fitting the b-wave data yielded half-saturating light intensities of $0.009 \pm 0.002$ cd · s m^{−2} (wild type, n = 7) and $0.34 \pm 0.04$ cd · s m^{−2} (Gngt1 [−/−], n = 7), and b-wave maximum amplitudes of $912 \pm 69$ μV (wild type, n = 7) and $821 \pm 50$ μV (Gngt1 [−/−], n = 7). Values are means ± SEM.

generated rotating sine wave gratings (Prusky et al., 2004) (Fig. 2A). The absolute contrast sensitivity of Gngt1 [−/−] mice was unaltered in the photopic region (−1 log cd m[−2] and brighter) where vision is maintained by cone photoreceptors (Umino et al., 2008) as rods become saturated. This result implies normal cone function and the absence of cone degeneration, consistent with the normal levels of cone M/L- and S-opsins and cone-specific transducin Gtα₂ subunit in Gngt1 [−/−] retinas (Fig. 1I) and the unaltered photopic ERG b-wave amplitudes (data not shown). In contrast, the scotopic (rod-mediated) spatial contrast sensitivity of Gtγ-deficient mice was shifted ∼100-fold to brighter light conditions (Fig. 2B), indicating substantial rod desensitization in the absence of Gtγ. Gngt1 [−/−] rods still contributed to mouse vision as spatial contrast sensitivity of Gngt1 [−/−] mice was approximately twofold ($p < 0.05$) higher compared with that in Gtα-deficient (Gnat1 [−/−]) animals, where rods are not functional (Calvert et al., 2000). Thus, although Gtγ-deficient mice retained rod vision, their visual sensitivity under dim light conditions was severely reduced.

The effect of Gtγ deletion on retinal function was further assessed by full-field ERGs. In agreement with our behavioral results, the scotopic visual sensitivity of 2-month-old Gngt1 [−/−] animals was markedly reduced compared with wild-type age-matched controls (Fig. 2C). The sensitivity of the photoreceptor-driven a-wave in Gngt1 [−/−] mice was greatly decreased (by ∼33-fold), and its maximal amplitude was also ∼2-fold smaller compared with wild-type animals (Fig. 2D, left). The reduction in amplitude of the scotopic b-wave, dominated by rod bipolar cells, in Gngt1 [−/−] animals was less dramatic (∼10%), but the b-wave sensitivity was decreased by ∼38-fold (Fig. 2D, right), in a reasonable agreement with the observed a-wave reduction. The latter result is in contrast to the 2600-fold reduction of b-wave sensitivity reported for the Deltagen Gngt1 [−/−] mice (Lobanova et al., 2008). Part of

this discrepancy is likely attributable to the significantly higher b-wave sensitivity in 1-month-old wild-type controls in the study by Lobanova et al. (2008) compared with that obtained by us and others for b-wave in 2- to 3-month-old wild-type mice (Brantley et al., 2008; Herrmann et al., 2010; Kolesnikov et al., 2010). In addition, the severe early retinal degeneration of the Deltagen Gngt1 [−/−] mice could have contributed to the large reduction of their b-wave responses, driven primarily by the bipolar cells.

### Reduced amplification of phototransduction cascade in Gtγ-deficient mice

The effect of Gtγ deletion and the accompanying approximately sixfold reduction of Gtα (Fig. 1H) on the rod phototransduction in individual mouse rods was analyzed by suction electrode recordings (Fig. 3). In agreement with the similar length of their outer segments at the age of 2 months, wild-type, Gngt1 [+/−], and Gngt1 [−/−] rods produced saturated responses of similar amplitudes (Fig. 3A, Table 1). The light sensitivity of Gngt1 [+/−] rods was decreased by only 1.4-fold compared with wild-type rods, consistent with a previous study (Herrmann et al., 2010). However, the sensitivity of Gngt1 [−/−] rods was reduced dramatically (90-fold) (Fig. 3B, Table 1).

To establish the reason for the reduced sensitivity in Gngt1 [−/−] rods, we evaluated the amplification of their phototransduction cascade by directly comparing the light intensities required to produce identical response activation phases (Fig. 3C). The phototransduction gain in wild-type and Gngt1 [+/−] rods was identical, as evident from the similar rising phases of their dim flash responses to the same flash intensity during the first 40 ms. In contrast, a matching rising phase for Gngt1 [−/−] rod responses required a 40-fold increase in flash strength. Taking into account low-pass filtering of the recordings, this translated into ∼33-fold reduction in phototransduction amplification of
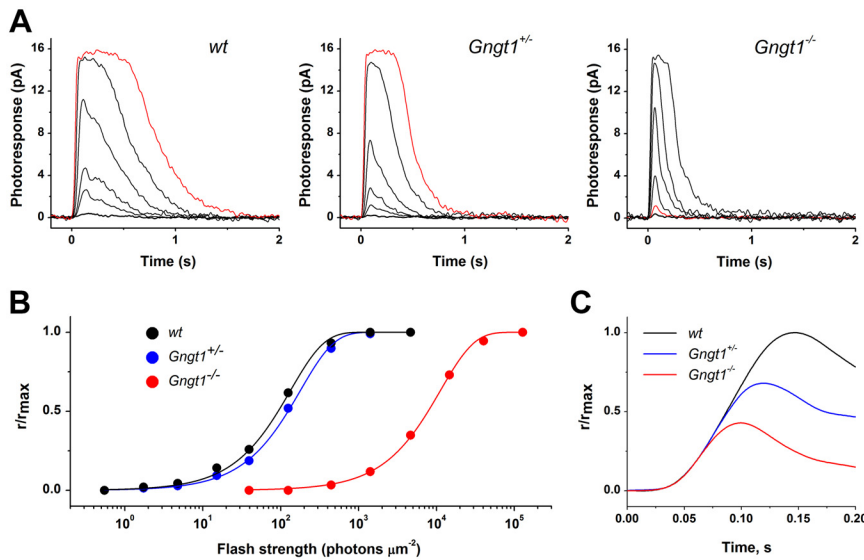
**Figure 3.** Light responses of control and Gt$\gamma$-deficient mouse rods. **A**, Representative families of flash responses from 2-month-old wild-type (left), Gngt1 $^{+/-}$ (middle), and Gngt1 $^{-/-}$ (right) mouse rods. Test flashes of 500 nm light with intensities of 5, 15, 39, 125, 444, and 1406 photons $\mu m^{-2}$ (for wild-type and Gngt1 $^{+/-}$ rods), or 444, 1406, 4630, 14,670, 40,440, and 128,160 photons $\mu m^{-2}$ (for Gngt1 $^{-/-}$ rods) were delivered at time 0. The red traces show responses to identical light intensity (1406 photons $\mu m^{-2}$). **B**, Normalized averaged intensity–response functions. Data were fitted with saturating exponential functions that yielded half-saturating light intensities of 93, 130, and 8408 photons $\mu m^{-2}$ for wild-type (n = 50), Gngt1 $^{+/-}$ (n = 27), and Gngt1 $^{-/-}$ (n = 41) mouse rods, respectively (see Table 1). Error bars (SEM) are smaller than the symbol size. **C**, Phototransduction cascade amplification in mouse rods. Population-averaged dim flash responses to light intensities corresponding to 15 photons $\mu m^{-2}$ for wild-type and Gngt1 $^{+/-}$ rods and 1406 photons $\mu m^{-2}$ for Gngt1 $^{-/-}$ rods were normalized to their corresponding maximum dark currents, $r_{max}$. Then the Gngt1 $^{+/-}$ and Gngt1 $^{-/-}$ responses were scaled to make the initial parts of all three responses to coincide. Correspondingly scaled light intensities were 1:1:0.025 (wild type:Gngt1 $^{+/-}$:Gngt1 $^{-/-}$). A slight response shift of 3 ms (Gngt1 $^{+/-}$) and 5 ms (Gngt1 $^{-/-}$) to longer times compared with wild-type rods was necessary, mostly caused by the low-pass filtering of the recordings.
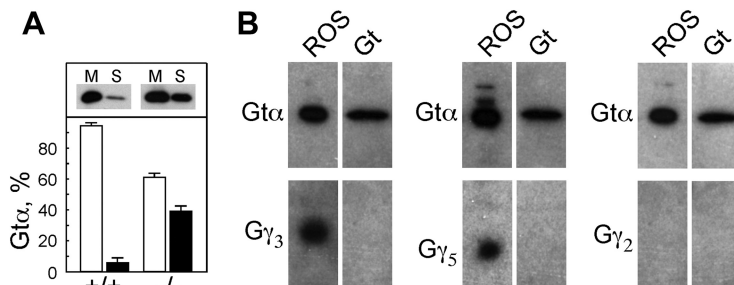


**Figure 4.** Interaction of Gt$\alpha$ with R* and analysis of purified Gt for the presence of several G$\gamma$ subunits. **A**, Gt$\alpha$ interactions with photoactivated ROS disk membranes. Top, Representative Western blot of the membrane (M) and soluble (S) fractions using anti-Gt$\alpha$ antibodies. Bottom, Corresponding densitometry results for the Gt$\alpha$ bands. Experimental conditions were as follows: 3 $\mu M$ rhodopsin, medium ionic strength buffer, 100% bleach, 4°C. All values are means ± SEM (n = 3). **B**, Western blot analysis of Gt purified from photoactivated washed Gngt1 $^{-/-}$ ROS disk membranes. Shown are the starting (crude, left) ROS sample (0.6 $\mu g$) and the final purified Gt sample (right). The top portion was stained with anti-Gt$\alpha$ antibody; the bottom portions were stained with anti-G$\gamma_3$, anti-G$\gamma_5$, and anti-G$\gamma_2$ antibodies.

Gngt1 $^{-/-}$ rods. Thus, although Gt$\gamma$-deficient rods were still able to respond to light, their sensitivity was severely reduced mostly because of a decrease in the amplification of their phototransduction cascade.

### Reduced affinity of Gt$\alpha$ toward R* in Gt$\gamma$-deficient mice

To determine the mechanism leading to the reduced amplification in Gngt1 $^{-/-}$ rods, we investigated whether the absence of Gt$\beta\gamma$ affects the binding efficiency of mouse Gt$\alpha$ to R* in ROS disk membranes purified from wild-type and Gngt1 $^{-/-}$ retinas. We performed biochemical measurements of endogenous Gt$\alpha$

interactions with photoactivated ROS disk membranes (characterized in Fig. 1) diluted to 3 $\mu M$ R* in medium ionic strength buffer (Kühn, 1980). In wild-type ROS disks containing native levels of Gt$\beta\gamma$, light induced binding of >90% of Gt$\alpha$ in the sample to R* membranes (Fig. 4A). In contrast, the lack of Gt$\beta\gamma$ resulted in reduced affinity of Gt$\alpha$ toward R* so that only ~60% of Gt$\alpha$ was bound to light-activated Gngt1 $^{-/-}$ ROS membranes (Fig. 4A).

Despite the severe defect in visual signal amplification and drastic reduction of light sensitivity, under brighter light Gngt1 $^{-/-}$ rods were still capable of producing responses with maximal amplitude similar to that in wild-type rods (Fig. 3). Whether this residual signaling is achieved by the monomeric Gt$\alpha$ or unknown heterotrimeric form of G-proteins is of considerable interest. Previous attempts to identify residual G$\gamma$ subunits in Deltagen Gngt1 $^{-/-}$ retinas did not reveal any G-protein heterotrimers that may exist in rods in addition to Gt. Yet, based on functional arguments (comparable reductions in ROS Gt$\alpha$ and in the rate of Gt$\alpha$ activation) and similar amounts of Gt$\alpha$ and Gt$\beta$ in ROS, it was suggested that signaling in the Deltagen Gngt1 $^{-/-}$ rods was likely to be mediated by the heterotrimeric G-protein containing an unknown G$\gamma$ (Lobanova et al., 2008). The direct protein quantification in our mice shows the presence of 17% of membrane-bound Gt$\alpha$ and 10% of Gt$\beta$ in Gngt1 $^{-/-}$ ROS disk membranes (Fig. 1G,H). Taking into consideration that the stoichiometry of Gt$\alpha$/Gt$\beta$/Gt$\gamma$ in the heterotrimeric complex is always 1:1:1, this result indicates that a substantial fraction of the Gt$\alpha$ pool in our G$\gamma$-deficient rods is monomeric. Because our ROS membranes contained residual G$\gamma_3$ and G$\gamma_5$ subunits (Fig. 1I), the remaining Gt$\alpha$ pool may have formed mixed Gt$\alpha\beta\gamma_{3/5}$ complexes. To determine whether these complexes exist in mutant ROS, we purified Gt using extensive washes of bleached Gngt1 $^{-/-}$ ROS membranes followed by a final GTP$\gamma$S elution step. Although G$\gamma_3$ and G$\gamma_5$ were clearly detectable in Gngt1 $^{-/-}$ ROS samples, no G$\beta\gamma$ subunits copurified with Gt$\alpha$ (Fig. 4B), providing a strong argument that G$\gamma_3$ and G$\gamma_5$ are trace contaminants and that the major pool of Gt$\alpha$ in Gngt1 $^{-/-}$ ROS is monomeric. However, as our detection method relies on immunoreactivity and possesses limited sensitivity, we cannot rule out that some fraction of Gt$\alpha$ is in heterotrimeric form of unknown composition. Whether the residual Gt$\alpha$ pool in our G$\gamma$-deficient rods signals as a monomer or in a combination with a G$\beta\gamma$ subunit, the reduction in gain of Gngt1 $^{-/-}$ rods clearly demonstrates that the Gt$\beta\gamma$ complex is indispensable for G-protein-mediated signal amplification.
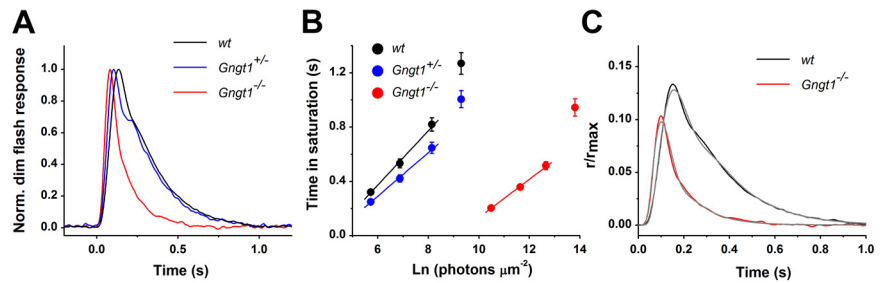
## Accelerated photoresponse inactivation in Gt$\gamma$-deficient rods

Surprisingly, there was a substantial difference between the ~90-fold reduction in rod sensitivity and the 33-fold reduction in amplification of phototransduction in *Gngt1*$^{-/-}$ rods. One possible explanation for this threefold difference could be faster inactivation of the transduction cascade in Gt$\gamma$-deficient rods, which would result in smaller light responses (hence lower sensitivity) than in wild-type rods. Indeed, the inactivation rate of dim flash photoresponses was significantly accelerated in *Gngt1*$^{-/-}$ rods (Fig. 5 *A*,*B*; Table 1). Two major inactivation processes, the rhodopsin shutoff and transducin inactivation, might be acceler-



**Figure 5.** Phototransduction cascade inactivation in control and Gt$\gamma$-deficient mouse rods. *A*, Normalized population-averaged dim flash responses (to light intensities of 15 photons $\mu$m$^{-2}$ for wild-type and *Gngt1*$^{+/-}$ rods and 1406 photons $\mu$m$^{-2}$ for *Gngt1*$^{-/-}$ rods) demonstrating the accelerated photoresponse inactivation in G$\gamma$-deficient rods. *B*, Determination of the dominant recovery time constant ($\tau_D$) from a series of supersaturating flashes. Linear fits throughout the data yielded $\tau_D$ values indicated in Table 1. Values are means ± SEM. *C*, Simulations of wild-type and *Gngt1*$^{-/-}$ rod responses with a mathematical model of mouse rod phototransduction (Kuzmin et al., 2004). The gray traces show model responses superimposed on experimental curves. For parameters of fitting, see Tables 1 and 2.

ated in our mutant cells. To evaluate these possibilities, we applied a mathematical model of the rod phototransduction (Kuzmin et al., 2004) (Fig. 5*C*; Tables 1, 2) (for detailed description of the model, see Materials and Methods).

The model parameters that were allowed to vary among strains of mice were only those whose values are critical for the sensitivity and kinetics of the response. They include the rate of activation of PDE by R* ($\nu_{RE}$), rates of rhodopsin ($k_{Rmax}$, $k_{Rmin}$) and phosphodiesterase ($k_E$) turnoff, and parameters of Ca$^{2+}$ buffering that define the kinetics of Ca$^{2+}$ feedback. An additional requirement was that the set of parameters providing a good fit to dim flash responses also ensured correct saturation times at bright flashes. Together, these restrictions greatly limited the freedom of fitting. Final sets of parameters allowed not more than a few percentage change in each value without markedly worsening the fit statistics. Under the restrictions discussed above, it was possible to faithfully reproduce wild-type, *Gngt1*$^{+/-}$, and *Gngt1*$^{-/-}$ responses by only varying $\nu_{RE}$, $k_E$, $k_{Rmax}$, and the buffering power of the ROS cytoplasm, FB (Fig. 5*C*, Table 1). Model responses to saturating flashes also correctly predicted time in saturation at the lowest flash strengths. In addition to a 33-fold reduction of amplification ($\nu_{RE}$) compared with wild-type controls, reproducing the *Gngt1*$^{-/-}$ rod responses required an increase in the rate of transducin/PDE inactivation ($k_E$) by a factor of ~1.33 and acceleration of rhodopsin turnoff ($k_{Rmax}$) by a factor of ~5.6. It was also necessary to accelerate Ca feedback (reduce FB) (Table 1) by approximately twofold in *Gngt1*$^{-/-}$ and *Gngt1*$^{+/-}$ rods. Thus, our model identified the acceleration of rhodopsin shutoff as the main cause for the faster response inactivation in *Gngt1*$^{-/-}$ rods.

## Discussion

To address the physiological role of transducin Gt$\beta\gamma$ complex in phototransduction, we generated mice lacking the rod-specific Gt$\gamma$ subunit (*Gngt1*$^{-/-}$). In stark contrast to a previous Deltagen Gt$\gamma$ knock-out model (Lobanova et al., 2008), the lack of early retinal degeneration and the normal expression levels of most transduction proteins in our mice (Fig. 1) allowed us to quantitatively characterize how the deletion of Gt$\gamma$ affects their visual function and phototransduction properties of individual rods. At all functional levels studied, *Gngt1*$^{-/-}$ mice consistently displayed impaired rod function and dramatic reduction in their scotopic light sensitivity (Figs. 2, 3). By using single-cell recordings, we identified a ~33-fold reduction in amplification of the phototransduction cascade in *Gngt1*$^{-/-}$ rods as the main cause

for their reduced photosensitivity (Fig. 3*C*). As amplification in mammalian rods is directly proportional to the level of Gt$\alpha$ subunit (Sokolov et al., 2002), only 6-fold of its reduction could be explained by the 17% Gt$\alpha$ bound to ROS disk membranes in *Gngt1*$^{-/-}$ rods compared with wild-type controls (Fig. 1*H*).

What is the explanation for the remaining (33/6 = 5.5-fold) reduction in rod amplification in the absence of Gt$\beta\gamma$? The use of brighter light to elicit photoresponses in *Gngt1*$^{-/-}$ rods would not be expected to affect their gain (Kahlert et al., 1990). Instead, the additional 5.5-fold decrease in the phototransduction amplification in *Gngt1*$^{-/-}$ rods should be attributed to the lack of the Gt$\beta\gamma$ complex. This conclusion is in striking contrast to that reached from the analysis of the Deltagen *Gngt1*$^{-/-}$ mouse (Lobanova et al., 2008), ascribing all reduction in light sensitivity to the reduced level of Gt$\alpha$ in its rapidly degenerating rods. Our conclusion about the crucial role of Gt$\beta\gamma$ in signal amplification would be unaffected by any residual signaling mechanisms, such as by a possible expression of cone Gt$\alpha$/Gt$\gamma$ in mouse rods (Allen et al., 2010). Any contribution from the small and desensitized *Gnat1*-independent rod responses observed in that study would be negligible in our single-cell recordings. Moreover, our attribution of 5.5-fold reduction of amplification in *Gngt1*$^{-/-}$ rods to the lack of Gt$\beta\gamma$ is only a lower estimate of its effect on Gt$\alpha$ activation. If unknown G$\beta\gamma$ complexes contribute to *Gngt1*$^{-/-}$ rod photoresponse, the actual efficiency of G$\beta\gamma$-devoid Gt$\alpha$ might be even lower than 1/5.5 of that of normal heterotrimer.

The crucial role for Gt$\beta\gamma$ in boosting phototransduction amplification in intact rods revealed in our study is in agreement with previous biochemical data showing the reduced ability of R* to activate monomeric bovine rod Gt$\alpha$, compared with the Gt heterotrimer (Navon and Fung, 1987; Phillips et al., 1992; Kisselev et al., 1999; Marin et al., 2000; Herrmann et al., 2006). However, the physiological relevance of such *in vitro* findings has been a long-standing question because R and Gt concentrations typically used in these studies were 3 orders of magnitude below those found in intact photoreceptors. In addition, it has been difficult to completely exclude the possibility that small Gt$\beta\gamma$ contamination in purified ROS membranes or Gt$\alpha$ could exaggerate the activity of monomeric Gt$\alpha$. Furthermore, other biochemical experiments contradicted these findings and suggested that, at bleached rhodopsin concentrations >1 $\mu$M, there appears to be no requirement for Gt$\beta\gamma$ in the Gt$\alpha$ activation event (Phillips et al., 1992).

Our biochemical measurements of endogenous Gt$\alpha$ interactions with photoactivated wild-type mouse ROS disk membranes

(Fig. 4$A$) demonstrated light-induced binding of >90% of Gt$\alpha$ to R* (Kühn, 1980; Fukada et al., 1990; Bigay et al., 1994; Herrmann et al., 2006). In contrast, the lack of Gt$\beta\gamma$ resulted in reduced affinity of Gt$\alpha$ toward R* so that only ~60% of Gt$\alpha$ was bound to light-activated $Gngt1^{-/-}$ ROS membranes, in agreement with previous data on monomeric Gt$\alpha$ (Phillips et al., 1992; Willardson et al., 1993; Matsuda et al., 1994). This value is in line with ~40% binding of purified bovine Gt$\alpha$ to light-activated membranes measured by dynamic light scattering (Herrmann et al., 2006). Although the soluble Gt$\alpha$ pool is fully capable of productive interactions with R*, the rate of its activation is limited by binding to the membrane and R* (Heck and Hofmann, 2001). This result is also consistent with a direct involvement of Gt$\beta\gamma$ in R* interactions and R*-catalyzed nucleotide exchange on Gt$\alpha$ (Kisselev and Downs, 2006; Katadae et al., 2008). Overall, this leads to the severely compromised rate of Gt$\alpha$ activation without Gt$\beta\gamma$. These biochemical studies, together with the physiological results presented here, demonstrate that in the absence of Gt$\beta\gamma$ R* activates Gt$\alpha$ at a substantially reduced rate, dramatically impairing the first step of signal amplification in rods. The resulting loss of light sensitivity in $Gngt1^{-/-}$ mice is in line with desensitization in invertebrates due to mutations in *Drosophila* G$\beta$e (Dolph et al., 1994), as well as in the farnesylation site of G$\gamma$e (Schillo et al., 2004), which prevents binding of G$\gamma$e to the membrane, suggesting a universal role of G$\beta\gamma$ complexes in controlling intracellular signal amplification.

Surprisingly, the inactivation rate of dim flash photoresponses was significantly accelerated in $Gngt1^{-/-}$ rods compared with wild-type photoreceptors (Fig. 5$A$,$B$; Table 1). To evaluate the two possibilities for accelerated response shutoff in mutant cells, the faster rhodopsin turnoff and/or faster transducin inactivation, a mathematical model of rod phototransduction (Kuzmin et al., 2004) was applied. It is believed that the rate of Gt$\alpha$-GTP/PDE inactivation by the RGS9/G$\beta$5/R9AP GAP complex ($k_E$ in the model) shapes the tail of the decay phase of dim flash responses and controls the recovery time of saturated responses in mice (Krispel et al., 2006; Burns and Pugh, 2009). In accordance with this idea, both inactivation time constants ($\tau_{rec}$ and $\tau_D$) were reduced in $Gngt1^{-/-}$ rods (Fig. 5$A$,$B$; Table 1). Modeling revealed a similar increase in $k_E$, indicating accelerated inactivation of Gt$\alpha$-GTP/PDE in Gt$\gamma$-deficient rods (Table 1). We found that levels of RGS9, G$\beta$5, PDE$\alpha$, and PDE$\beta$ subunits were unaffected by the deletion of Gt$\gamma$ (Fig. 1$I$). At first glance, the sixfold reduction in Gt$\alpha$ in $Gngt1^{-/-}$ rods could possibly accelerate their response inactivation by increasing the ratio of RGS9/Gt$\alpha$. However, RGS9 is known to interact only with the activated form of Gt$\alpha$, Gt$\alpha$-GTP. Because our test flashes produced responses of similar amplitudes in wild-type and $Gngt1^{-/-}$ rods, they also would be expected to produce similar amounts of Gt$\alpha$-GTP, preserving the RGS9/Gt$\alpha$-GTP ratio. Thus, the inactivation of Gt$\alpha$-GTP/PDE is unlikely to be accelerated in Gt$\gamma$-deficient rods because of the reduced level of Gt$\alpha$.

Acceleration of the response shutoff can be also achieved by adding an excess PDE$\gamma$ subunit by either its overexpression in mouse rods (Tsang et al., 2006) or its infusion in toad ROSs (Rieke and Baylor, 1996). Although the mechanism of this effect remains unclear, it provides a possible connection between the acceleration of response shutoff and our finding that expression of the inhibitory PDE$\gamma$ subunit is upregulated by twofold and threefold in $Gngt1^{+/-}$ and $Gngt1^{-/-}$ ROS, respectively (Fig. 1$I$). Notably, $Gngt1^{+/-}$ rods displayed both an intermediate level of PDE$\gamma$ expression and an intermediate rate of photoresponse turnoff (Fig. 5$A$,$B$; Table 1), whereas the rising phase of their

response (amplification) was identical with that in wild-type photoreceptors (Fig. 3$C$, Table 1).

Finally, one important conclusion from our modeling of mouse phototransduction was a substantially faster rate of rhodopsin inactivation ($k_{Rmax}$) in Gt$\gamma$-deficient rods. As indicated above, in our model this effect was substantially more prominent than the acceleration of $k_E$. The lowest estimate of R* turnoff acceleration compatible with the observed kinetics of $Gngt1^{-/-}$ responses was approximately threefold. Such acceleration of rhodopsin shutoff could potentially be caused by a relief of competition between rhodopsin kinase (GRK1), arrestin1 (Arr1), and Gt for photoactivated pigment (Doan et al., 2009), because of the partial overlapping of their binding sites on the cytoplasmic domains of R* (König et al., 1989; Krupnick et al., 1997; Raman et al., 1999; Gurevich and Gurevich, 2006). In this scenario, the reduced level of Gt$\alpha$ (Fig. 1$H$), together with the 5.5-fold lower efficiency of Gt$\alpha$ interaction with R*, could enable both GRK1 and Arr1 (whose levels were unaltered in $Gngt1^{-/-}$ retinas) (Fig. 1$I$) to quench R* faster. However, the fact that the rate of phototransduction activation is proportional to Gt concentration (Sokolov et al., 2002) shows that R* mostly exists in a free form rather than as R*-Gt$\alpha$($\beta\gamma$) complex. Therefore, Gt$\alpha$($\beta\gamma$) cannot apparently outcompete GRK1 and Arr1, even in wild-type rods. Additional experiments are necessary to find the cause(s) of faster R* shutoff in our $Gngt1^{-/-}$ mice.

Universal mechanisms of intracellular signal transduction and amplification enable cells to detect and respond to very faint environmental signals. Our results obtained in intact mammalian rod photoreceptor cells address the role of the G-protein $\beta\gamma$-complex in modulating visual signaling. Investigating the function of G$\gamma$-deficient rods, we demonstrate that heterotrimeric G-proteins are best suited for the task: although G$\alpha$ is sufficient for signal transduction, the efficient signal amplification required for nocturnal vision is achieved in the presence of the G$\beta\gamma$ complex. This highlights a unique role of G$\gamma$, and more broadly of G$\beta\gamma$ complexes, in regulating the amplification of visual signals in phototransduction.

## References

Allen AE, Cameron MA, Brown TM, Vugler AA, Lucas RJ (2010) Visual responses in mice lacking critical components of all known retinal phototransduction cascades. PLoS One 5:e15063.

Baylor DA, Lamb TD, Yau KW (1979) Responses of retinal rods to single photons. J Physiol 288:613–634.

Bigay J, Faurobert E, Franco M, Chabre M (1994) Roles of lipid modifications of transducin subunits in their GDP-dependent association and membrane binding. Biochemistry 33:14081–14090.

Brantley MA Jr, Jain S, Barr EE, Johnson EM Jr, Milbrandt J (2008) Neurturin-mediated ret activation is required for retinal function. J Neurosci 28:4123–4135.

Burns ME, Pugh EN Jr (2009) RGS9 concentration matters in rod phototransduction. Biophys J 97:1538–1547.

Burns ME, Mendez A, Chen J, Baylor DA (2002) Dynamics of cyclic GMP synthesis in retinal rods. Neuron 36:81–91.

Calvert PD, Ho TW, LeFebvre YM, Arshavsky VY (1998) Onset of feedback reactions underlying vertebrate rod photoreceptor light adaptation. J Gen Physiol 111:39–51.

Calvert PD, Krasnoperova NV, Lyubarsky AL, Isayama T, Nicoló M, Kosaras B, Wong G, Gannon KS, Margolskee RF, Sidman RL, Pugh EN Jr, Makino CL, Lem J (2000) Phototransduction in transgenic mice after targeted deletion of the rod transducin alpha-subunit. Proc Natl Acad Sci U S A 97:13913–13918.

Cervetto L, Lagnado L, Perry RJ, Robinson DW, McNaughton PA (1989) Extrusion of calcium from rod outer segments is driven by both sodium and potassium gradients. Nature 337:740–743.

Doan T, Azevedo AW, Hurley JB, Rieke F (2009) Arrestin competition in-

fluences the kinetics and variability of the single-photon responses of mammalian rod photoreceptors. J Neurosci 29:11867–11879.

Dolph PJ, Man-Son-Hing H, Yarfitz S, Colley NJ, Deer JR, Spencer M, Hurley JB, Zuker CS (1994) An eye-specific G beta subunit essential for termination of the phototransduction cascade. Nature 370:59–61.

Downes GB, Gautam N (1999) The G protein subunit gene families. Genomics 62:544–552.

Fu Y, Yau KW (2007) Phototransduction in mouse rods and cones. Pflugers Arch 454:805–819.

Fukada Y, Takao T, Ohguro H, Yoshizawa T, Akino T, Shimonishi Y (1990) Farnesylated gamma-subunit of photoreceptor G protein indispensable for GTP-binding. Nature 346:658–660.

Fung BK (1983) Characterization of transducin from bovine retinal rod outer segments. I. Separation and reconstitution of the subunits. J Biol Chem 258:10495–10502.

Govardovskii VI, Kuzmin DG (1999) Light-induced calcium release and kinetics of calcium feedback in retinal rods. Sensory Systems (Russian) 13:213–222.

Gurevich VV, Gurevich EV (2006) The structural basis of arrestin-mediated regulation of G-protein-coupled receptors. Pharmacol Ther 110:465–502.

Hamer RD (2000a) Computational analysis of vertebrate phototransduction: combined quantitative and qualitative modeling of dark- and light-adapted responses in amphibian rods. Vis Neurosci 17:679–699.

Hamer RD (2000b) Analysis of $Ca^{++}$-dependent gain changes in PDE activation in vertebrate rod phototransduction. Mol Vis 6:265–286.

Hamer RD, Nicholas SC, Tranchina D, Liebman PA, Lamb TD (2003) Multiple steps of phosphorylation of activated rhodopsin can account for the reproducibility of vertebrate rod single-photon responses. J Gen Physiol 122:419–444.

Hamer RD, Nicholas SC, Tranchina D, Lamb TD, Jarvinen JL (2005) Toward a unified model of vertebrate rod phototransduction. Vis Neurosci 22:417–436.

Heck M, Hofmann KP (2001) Maximal rate and nucleotide dependence of rhodopsin-catalyzed transducin activation: initial rate analysis based on a double displacement mechanism. J Biol Chem 276:10000–10009.

Herrmann R, Heck M, Henklein P, Hofmann KP, Ernst OP (2006) Signal transfer from GPCRs to G proteins: role of the G alpha N-terminal region in rhodopsin-transducin coupling. J Biol Chem 281:30234–30241.

Herrmann R, Lobanova ES, Hammond T, Kessler C, Burns ME, Frishman LJ, Arshavsky VY (2010) Phosducin regulates transmission at the photoreceptor-to-ON-bipolar cell synapse. J Neurosci 30:3239–3253.

Hurley JB, Fong HK, Teplow DB, Dreyer WJ, Simon MI (1984) Isolation and characterization of a cDNA clone for the gamma subunit of bovine retinal transducin. Proc Natl Acad Sci U S A 81:6948–6952.

Kahlert M, Pepperberg DR, Hofmann KP (1990) Effect of bleached rhodopsin on signal amplification in rod visual receptors. Nature 345:537–539.

Katadae M, Hagiwara K, Wada A, Ito M, Umeda M, Casey PJ, Fukada Y (2008) Interacting targets of the farnesyl of transducin gamma-subunit. Biochemistry 47:8424–8433.

Kisselev OG (2007) Photoactivation of rhodopsin and signal transfer to transducin. In: Signal transduction in the retina (Fliesler SJ, Kisselev OG, eds), pp 33–54. Boca Raton, FL: CRC.

Kisselev OG, Downs MA (2006) Rhodopsin-interacting surface of the transducin gamma subunit. Biochemistry 45:9386–9392.

Kisselev OG, Meyer CK, Heck M, Ernst OP, Hofmann KP (1999) Signal transfer from rhodopsin to the G-protein: evidence for a two-site sequential fit mechanism. Proc Natl Acad Sci U S A 96:4898–4903.

Kolesnikov AV, Fan J, Crouch RK, Kefalov VJ (2010) Age-related deterioration of rod vision in mice. J Neurosci 30:11222–11231.

König B, Arendt A, McDowell JH, Kahlert M, Hargrave PA, Hofmann KP (1989) Three cytoplasmic loops of rhodopsin interact with transducin. Proc Natl Acad Sci U S A 86:6878–6882.

Krispel CM, Chen D, Melling N, Chen YJ, Martemyanov KA, Quillinan N, Arshavsky VY, Wensel TG, Chen CK, Burns ME (2006) RGS expression rate-limits recovery of rod photoresponses. Neuron 51:409–416.

Krispel CM, Sokolov M, Chen YM, Song H, Herrmann R, Arshavsky VY, Burns ME (2007) Phosducin regulates the expression of transducin betagamma subunits in rod photoreceptors and does not contribute to phototransduction adaptation. J Gen Physiol 130:303–312.

Krupnick JG, Gurevich VV, Benovic JL (1997) Mechanism of quenching of

phototransduction. Binding competition between arrestin and transducin for phosphorhodopsin. J Biol Chem 272:18125–18131.

Kühn H (1980) Light- and GTP-regulated interaction of GTPase and other proteins with bovine photoreceptor membranes. Nature 283:587–589.

Kuzmin DG, Travnikov SV, Firsov ML, Govardovskii VI (2004) Mathematical model of phototransduction and light adaptation in frog retinal rods. Sensory Systems (Russian) 18:305–316.

Lagnado L, Cervetto L, McNaughton PA (1992) Calcium homeostasis in the outer segments of retinal rods from the tiger salamander. J Physiol 455:111–142.

Leskov IB, Klenchin VA, Handy JW, Whitlock GG, Govardovskii VI, Bownds MD, Lamb TD, Pugh EN Jr, Arshavsky VY (2000) The gain of rod phototransduction: reconciliation of biochemical and electrophysiological measurements. Neuron 27:525–537.

Lobanova ES, Finkelstein S, Herrmann R, Chen YM, Kessler C, Michaud NA, Trieu LH, Strissel KJ, Burns ME, Arshavsky VY (2008) Transducin $\gamma$-subunit sets expression levels of $\alpha$- and $\beta$-subunits and is crucial for rod viability. J Neurosci 28:3510–3520.

Marin EP, Krishna AG, Zvyaga TA, Isele J, Siebert F, Sakmar TP (2000) The amino terminus of the fourth cytoplasmic loop of rhodopsin modulates rhodopsin-transducin interaction. J Biol Chem 275:1930–1936.

Matsuda T, Takao T, Shimonishi Y, Murata M, Asano T, Yoshizawa T, Fukada Y (1994) Characterization of interactions between transducin alpha/beta gamma-subunits and lipid membranes. J Biol Chem 269:30358–30363.

McCarthy ST, Younger JP, Owen WG (1996) Dynamic, spatially nonuniform calcium regulation in frog rods exposed to light. J Neurophysiol 76:1991–2004.

Naash MI, Wu TH, Chakraborty D, Fliesler SJ, Ding XQ, Nour M, Peachey NS, Lem J, Qtaishat N, Al-Ubaidi MR, Ripps H (2004) Retinal abnormalities associated with the G90D mutation in opsin. J Comp Neurol 478:149–163.

Navon SE, Fung BK (1987) Characterization of transducin from bovine retinal rod outer segments. Participation of the amino-terminal region of T alpha in subunit interaction. J Biol Chem 262:15746–15751.

Nickell S, Park PS, Baumeister W, Palczewski K (2007) Three-dimensional architecture of murine rod outer segments determined by cryoelectron tomography. J Cell Biol 177:917–925.

Nikonov S, Lamb TD, Pugh EN Jr (2000) The role of steady phosphodiesterase activity in the kinetics and sensitivity of the light-adapted salamander rod photoresponse. J Gen Physiol 116:795–824.

Oldham WM, Hamm HE (2008) Heterotrimeric G-protein activation by G-protein-coupled receptors. Nat Rev Mol Cell Biol 9:60–71.

Papermaster DS, Dreyer WJ (1974) Rhodopsin content in the outer segment membranes of bovine and frog retinal rods. Biochemistry 13:2438–2444.

Pepperberg DR, Cornwall MC, Kahlert M, Hofmann KP, Jin J, Jones GJ, Ripps H (1992) Light-dependent delay in the falling phase of the retinal rod photoresponse. Vis Neurosci 8:9–18.

Phillips WJ, Wong SC, Cerione RA (1992) Rhodopsin/transducin interactions. II. Influence of the transducin-beta gamma subunit complex on the coupling of the transducin-alpha subunit to rhodopsin. J Biol Chem 267:17040–17046.

Prusky GT, Alam NM, Beekman S, Douglas RM (2004) Rapid quantification of adult and developing mouse spatial vision using a virtual optomotor system. Invest Ophthalmol Vis Sci 45:4611–4616.

Pugh EN Jr, Lamb TD (1993) Amplification and kinetics of the activation steps in phototransduction. Biochim Biophys Acta 1141:111–149.

Raman D, Osawa S, Weiss ER (1999) Binding of arrestin to cytoplasmic loop mutants of bovine rhodopsin. Biochemistry 38:5117–5123.

Rieke F, Baylor DA (1996) Molecular origin of continuous dark noise in rod photoreceptors. Biophys J 71:2553–2572.

Scherer SW, Feinstein DS, Oliveira L, Tsui LC, Pittler SJ (1996) Gene structure and chromosome localization to 7q21.3 of the human rod photoreceptor transducin gamma-subunit gene (GNGT1). Genomics 35:241–243.

Schillo S, Belusic G, Hartmann K, Franz C, Kühl B, Brenner-Weiss G, Paulsen R, Huber A (2004) Targeted mutagenesis of the farnesylation site of *Drosophila* Ggammae disrupts membrane association of the G protein betagamma complex and affects the light sensitivity of the visual system. J Biol Chem 279:36309–36316.

Sokolov M, Lyubarsky AL, Strissel KJ, Savchenko AB, Govardovskii VI, Pugh EN Jr, Arshavsky VY (2002) Massive light-driven translocation of trans-

ducin between the two major compartments of rod cells: a novel mechanism of light adaptation. Neuron 34:95–106.

Stryer L (1986) Cyclic GMP cascade of vision. Annu Rev Neurosci 9:87–119.

Tao L, Pandey S, Simon MI, Fong HK (1993) Structure of the bovine transducin gamma subunit gene and analysis of promoter function in transgenic mice. Exp Eye Res 56:497–507.

Tsang SH, Woodruff ML, Chen CK, Yamashita CY, Cilluffo MC, Rao AL, Farber DB, Fain GL (2006) GAP-independent termination of photoreceptor light response by excess $\gamma$ subunit of the cGMP-phosphodiesterase. J Neurosci 26:4472–4480.

Umino Y, Solessio E, Barlow RB (2008) Speed, spatial, and temporal tuning of rod and cone vision in mouse. J Neurosci 28:189–198.

Wensel TG (2008) Signal transducing membrane complexes of photoreceptor outer segments. Vision Res 48:2052–2061.

Willardson BM, Pou B, Yoshida T, Bitensky MW (1993) Cooperative binding of the retinal rod G-protein, transducin, to light-activated rhodopsin. J Biol Chem 268:6371–6382.

Yatsunami K, Pandya BV, Oprian DD, Khorana HG (1985) cDNA-derived amino acid sequence of the gamma subunit of GTPase from bovine rod outer segments. Proc Natl Acad Sci U S A 82:1936–1940.

Younger JP, McCarthy ST, Owen WG (1996) Light-dependent control of calcium in intact rods of the bullfrog *Rana catesbeiana*. J Neurophysiol 75:354–366.

Zhu X, Brown B, Li A, Mears AJ, Swaroop A, Craft CM (2003) GRK1-dependent phosphorylation of S and M opsins and their binding to cone arrestin during cone phototransduction in the mouse retina. J Neurosci 23:6152–6160.